Spray Layer-by-Layer Assembled Clay Composite Thin Films as Selective Layers in Reverse Osmosis Membranes

*Jason R. Kovacs, Chaoyang Liu, Paula T. Hammond**

Department of Chemical Engineering, Massachusetts Institute of Technology, Cambridge, Massachusetts, 02139, United States

KEYWORDS: layer-by-layer, spray layer-by-layer, laponite clay, composite thin film, reverse osmosis membrane, nanofiltration membrane, water permeation, salt permeation

Abstract

Spray layer-by-layer assembled thin films containing laponite (LAP) clay exhibit effective salt barrier and water permeability properties when applied as selective layers in reverse osmosis (RO) membranes. Negatively-charged LAP platelets were layered with poly(diallyldimethylammonium) (PDAC), poly(allylamine) (PAH), and poly(acrylic acid) (PAA) in bilayer and tetralayer film architectures to generate uniform films on the order of 100 nm thick that bridge a porous polyethersulfone support to form novel RO membranes. Nanostructures were formed of clay layers intercalated in a polymeric matrix that introduced size-exclusion transport mechanisms into the selective layer. Thermal cross-linking of the polymeric matrix can

be used to increase the mechanical stability of the films and improve salt rejection by constraining swelling during operation. Maximum salt rejection of 89% was observed for the tetralayer film architecture, with an order of magnitude increase in water permeability compared to commercially available TFC-HR membranes. These clay composite thin films could serve as a high-flux alternative to current polymeric RO membranes for wastewater and brackish water treatment as well as potentially for forward osmosis applications. In general, we illustrate that by investigating the composite systems accessed using alternating layer-by-layer assembly in conjunction with complementary covalent crosslinking, it is possible to design thin film membranes with tunable transport properties for water purification applications.

Introduction

The Earth's surface is dominated by oceans, seas, and glaciers, but geological surveys indicate only 0.8% of these water resources meet the minimum standard for freshwater adequate for human consumption[1]. Additionally, agriculture and poor irrigation practices[2-3], mining operations[4-6], industrial production[7-8], and other human activity[9] can produce significant amounts of wastewater that must be treated before it can be reused or discharged to the environment without a significant ecological impact. Efficient water desalination is already is vital and will continue to be to sustain the quality of life for societies living without sufficient access to freshwater.

Membrane processes, the most commonly implemented being reverse osmosis (RO)[10], are playing a larger role in desalination because the energy costs per volume of freshwater produced are an order of magnitude lower than the costs associated with thermal desalting processes[11-12]. In RO, water is desalted via pressurized flow past a salt-selective membrane

which produces two product streams: a desalted permeate stream and a retentate stream of concentrated brine. Although RO has been proven to be a robust process, challenges remain to fully optimize RO membranes to increase throughput and lower power consumption. These challenges may be addressed by manipulating the structure and composition of the RO membrane[10, 13]. Currently, state-of-the-art thin film composite RO membranes are comprised of two or more layers: 1) a dense polyamide selective layer deposited through interfacial polymerization that accomplishes the separation, 2) a polysulfone or polyethersulfone support layer to provide a mechanically robust, porous support for the selective layer, and optionally 3) polyester or other backing materials for mounting the RO membrane into an appropriate module[14].

While a number of transport mechanisms can partially describe the flux of solvated ions and water through the selective layer, the exact mechanism is the subject of debate. It is generally accepted that solvated ions diffuse at a slower rate than water molecules through the polymer matrix[15]. The rate of diffusion through a dense polymer layer is a function of several factors, including the hydrodynamic radius of the molecule, the charge or lack thereof on the molecule, and environmental factors such as temperature and applied pressure that affect the activity and chemical potential of the molecules[16]. Note the hydrodynamic radius of a diffusing ion is not simply the radius of the ion or the polyatomic species, but also includes the shell of closely hydrogen-bonded water molecules around the ion, termed a solvated ion. The size of the solvation shell is a function of the attractive electrostatic forces between the ion and the oppositely-charged dipole of the water molecules and the repulsive forces between the nuclei[17-18]. These solvation shells increase the effective size of the solute to the order of a single nanometer for common monatomic ions like sodium and chloride to several nanometers for

larger polyatomic ions such as sulfates, with lighter monatomic ions being relatively larger than heavier monatomic ions due to the increased charge density[19-21].

There is an inverse relationship between salt rejection and water flux, and manipulating membrane properties such as the porosity of either the selective or support layer to maximize one desired attribute will reduce the other. To address this trade-off, researchers have investigated the use of nanostructured materials that enable less-hindered water transport while still providing mechanisms for salt rejection in the membrane[22]. The literature on nanostructured materials for RO membranes contains experimental and theoretical work on selective layers using carbon nanotubes[23], graphene[24], metal oxide nanoparticles[25-26], and zeolites[27] with varying degrees of success. Underlying these investigations is the hypothesis that the incorporation of impermeable nanomaterials into a selective layer introduces effective nano-sized channels inhibiting the flux of large solutes. Particularly, the focus is on developing channels or pores with a length scale on the order of 1 nm, which enables solute rejection *via* size exclusion[28], as this number is between the hydrodynamic radius of a water molecule and small solvated ions such as Na^+ and Cl^-[15]. For this reason, we are interested in the use of laponite clay, a high-aspect ratio nano-platelet that may be layered into films to form highly tortuous diffusive pathways for solvated ions. Clay-containing ceramic membranes have been used with some success in water microfiltration applications[29] and oil-water separations[30], while recent research into the use of similar composite thin films as selective layers in RO membranes has primarily focused on the incorporation of carbon nanotubes and zeolites[22]. More generally, polymer-clay composites have unique properties that have been utilized in a number of applications including gas barriers[31-34], medical devices and biocompatible materials[35-37], and the release of chemical agents[38].

Many of the assembly techniques commonly used to incorporate these nanomaterials into membranes, such as the inclusion of nanoparticles to the polymerization step of the selective layer or the phase inversion processing of the support layer, generate composites with a disordered internal structure that do not form uniform barrier layers. A potential improvement to this approach would be to build a more uniform selective layer through a sequential assembly process, enabling finer control over the internal structure of the selective layer. The layer-by-layer (LbL) assembly process, in which thin films are assembled via the sequential deposition of film components with complementary functionality such as electrostatic interactions[39], is one such method to accomplish this control while enabling the construction of highly conformal thin films atop a range of porous supports. The composition of LbL films can be varied through the manipulation of process conditions such as deposition times, concentration of the adsorbing solutions, and ionic strength of the film components[40-41]. Aerosolizing the film components with a forcing gas and spraying onto the substrate in what is termed Spray Layer-by-Layer (Spray-LbL) assembly can decrease the processing time for depositing large films by an order of magnitude[42] and further enhance the lateral order of nanomaterials incorporated in the film. Previous research has examined the use of LbL films containing polyelectrolytes[43-49] and metal-ion complexed polymers[50] has been conducted on dip-assembled and spin-assembled LbL films to serve as selective layers in osmotic membranes. The flexibility of the LbL assembly process enables the incorporation of clay platelets into LbL-assembled films[51-53], but there is a gap in the scientific literature concerning the use of LbL to generate nanostructured clay composite selective layers for RO membranes.

In this work, we investigate several spray-LbL assembled film architectures that consist of laponite clay layers (LAP) and polyelectrolyte layers. Analogous to what is observed in

models for composite polymer-clay membranes used in gas permeation applications[54], we hypothesize alternating layers of clay intercalated with polyelectrolytes will increase the tortuosity of the diffusive path length for solutes and introduce size-exclusive transport mechanisms that impact the transport of solvated ions to a greater degree than for smaller water molecules. We ground this hypothesis in three primary observations: first, prior work has shown laponite clay-containing thin films inhibit the in-plane mobility of Li^+ ions by up to two orders of magnitude compared to the cross-plane mobility, thus serving as a barrier to ion mobility[55]. Second, incorporation of clay platelets into polymer composites was found to significantly increase selectivity in gas barrier and separation membranes, showing that LbL-assembled clay composites serve as an effective small molecule barrier[31-34]. Third, recent studies on RO membranes containing inorganic nanoscale materials suggest the possibility of preferential water flow channels through the composite membrane[15]. Through tuning of the LbL assembly conditions, films can be assembled with a relatively high degree of incorporation of nanomaterial into the polymer matrix, on the order of 50% of the weight fraction of the film[56], compared to weight fractions under 10% observed in traditional polymer composites[57-58]. We believe an increased quantity of nanostructured materials can further enhance selectivity in RO membranes.

Results and Discussion

In this work, the spray-LbL assembly technique is used to deposit composite thin films containing LAP on polyethersulfone ultrafiltration membranes to generate novel RO membranes. LAP clay platelets were selected for the composite film assembly for three reasons. First, the cation-exchanged platelets have a negative surface charge and thus can be incorporated into LbL film architectures. Second, the platelets have a flat disc-like geometry with an aspect ratio of approximately 25:1[59] to 30:1[60], and can be layered into films aligned with the membrane surface

as shown in Figure 1. Three, LAP clay has a smaller particle size than other silicate clays such as montmorillonite, and thus is more compatible with the aerosolization technologies used in spray-LbL deposition. These features make LAP clay platelets ideal for the spray-LbL deposition of these types of clay composite thin films.

We examine two composite film architectures, the first containing the strong polycation poly(diallyldimethylammonium) (PDAC) and laponite (LAP) clay, shown in Figure 1a. For this film architecture, we control the composition of clay in the film by adjusting the spray times of the two film components. For the first film, the PDAC spray time was held constant at 3 seconds and the LAP clay spray time was held at 3 seconds (3s:3s); for the second bilayer composite film, the LAP clay spray time was increased to 9 seconds (3s:9s).

The second is a cross-linked tetralayer architecture of poly(allylamine) (PAH) and poly(acrylic acid) (PAA) bilayers between clay-containing bilayers of PAH and LAP, shown in Figure 1b. As both PAH and PAA are weak polyelectrolytes their degree of ionization depend on assembly pH. We examined films assembled at pH 5 and pH 6, which yield different film properties. Both the pH 5 and pH 6 films swell under aqueous conditions, as is expected for most LbL polyelectrolyte film systems, so thermal cross-linking[61] was used to form covalent bonds in the polymer matrix to lower film swelling. This additional step maintains the average spacing between layers of clay platelets to maintain an effective barrier layer, while toughening the polymer matrix and increasing the overall hardness and elastic modulus of the film, a phenomenon observed in prior research on polymer-clay nanocomposite films[62]. Finally, a cross-linked (PAH/PAA) film assembled at pH 5.0 without clay was used as a control system.

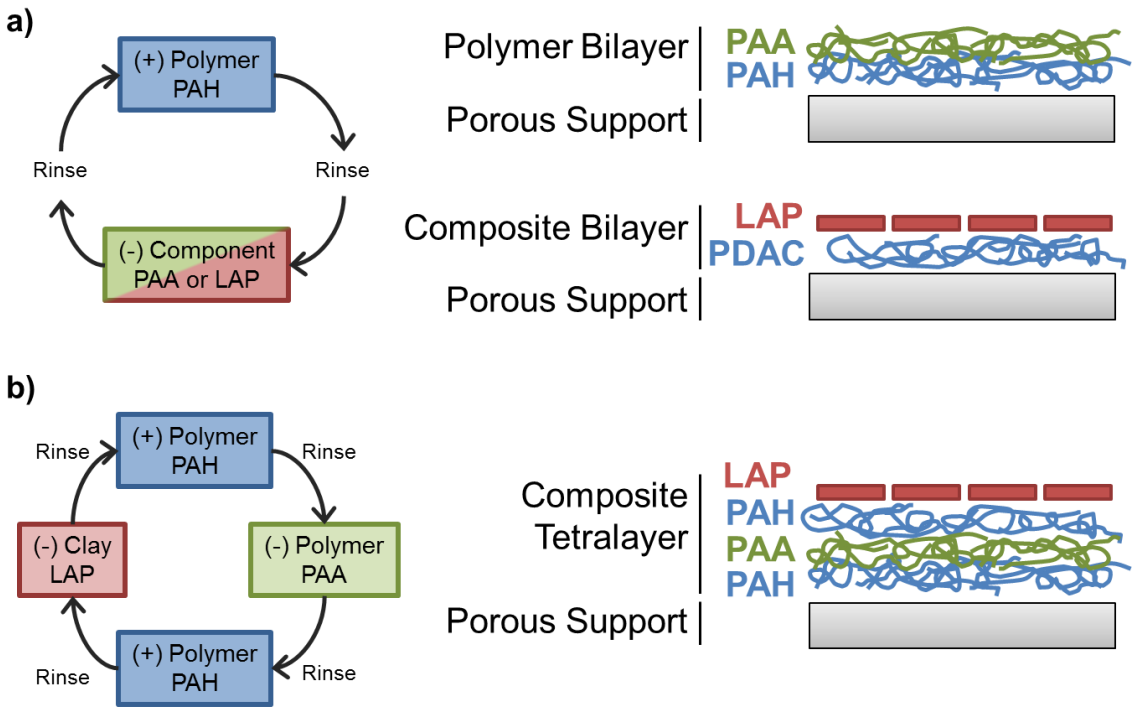

Figure 1. Spray-LbL assembly process and film architectures of a) polymer and composite bilayer films, and b) nanocomposite tetralayer films. Process is repeated to deposit desired number of bilayers or tetralayers.

Film Thickness and Composition. The dry thicknesses of the assembled thin films were measured by profilometry. All of the examined film architectures appear to grow linearly with respect to the number of bilayers or tetralayers deposited (Figure 2a and 2b) up to a maximum of 60 repeating units. The thickness per bilayer for the (PDAC/LAP) 3s:3s composite bilayer films was approximately 2.6 nm per bilayer, and for (PDAC/LAP) 3s:9s system 5.2 nm per bilayer, approximately 84% thicker. This corresponds to an increase in the clay content of the films from 52% at 3s:3s to 83% at 3s:9s (Table 1), indicating the increase in thickness is correlated with the additional incorporation of LAP into the film. The increase in clay content with longer spray times indicates that for these LAP containing film architectures, the spray-LbL

deposition does not achieve full equilibrium at the film interface per layer deposition. Rather, more clay is deposited at longer exposures, which suggests kinetic control of LbL film content over these spray conditions, in contrast to the equilibrium-controlled mass content usually observed with dip-LbL with appropriately long dipping times.

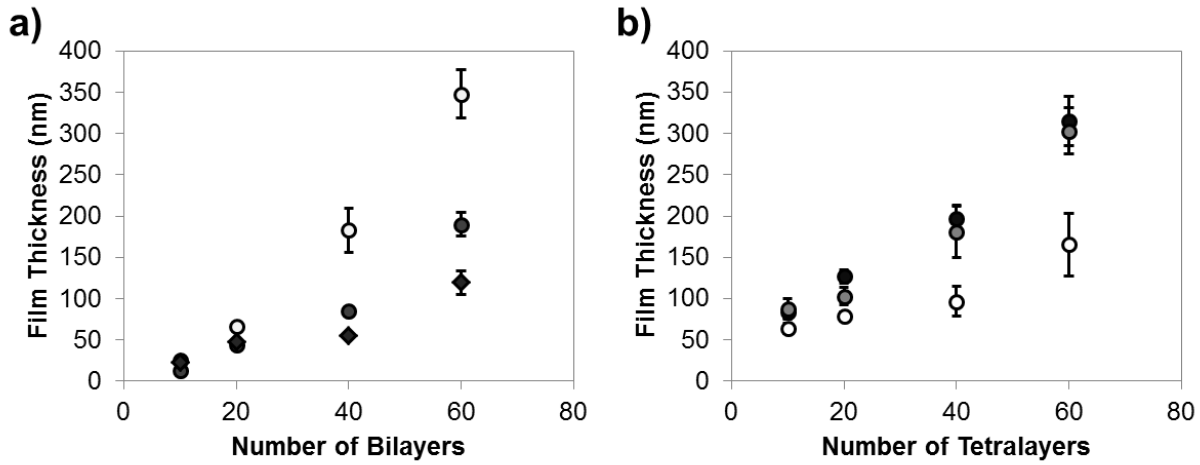

Figure 2. Growth curves of spray layer-by-layer assembled a) polymer bilayer (PAH/PAA) and composite (PDAC/LAP) thin films, and b) composite tetralayer (PAH/PAA/PAH/LAP) thin films assembled at different pH values.

Table 1. Film clay content as a function of assembly conditions

Film Architecture	*Clay Content (wt. %)*	*Thickness per Repeat Unit*
(PAH/PAA), pH 5.0	0%	1.5 nm/bl
(PDAC/LAP), 3s:3s	52.5% ± 6.9%	2.6 nm/bl
(PDAC/LAP), 3s:9s	82.6% ± 2.2%	5.2 nm/bl

(PAH/PAA/PAH/LAP), pH 5.0	37.8% ± 4.9%	5.0 nm/tl
(PAH/PAA/PAH/LAP), pH 6.0	56.3% ± 6.6%	2.6 nm/tl

The tetralayer films were assembled with spray times of 3 seconds maintained for each film component but at three assembly pH values. At pH 6.0, the PAH and PAA are both highly ionized when deposited at the film interface based on their respective pKa values (PAA pKa = 6.0-6.5; PAH pKa = 8.0-9.0[63]), which results in very thin, dense polymer layers being deposited. On average, the dry thickness for (PAH/PAA/PAH/LAP) pH 6.0 films was 2.6 nm per tetralayer, similar to what was observed for the (PDAC/LAP) 3s:3s assembly conditions (Figure 2b). The clay content of these two films were also statistically indistinguishable (Table 1), indicating the polymeric matrices of the (PDAC/LAP) 3s and (PAH/PAA/PAH/LAP) pH 6.0 films were of similar dry film thickness.

The (PAH/PAA/PAH/LAP) pH 5.0 and pH 5.5 films assembled were significantly thicker than the pH 6.0 films of the same architecture, with a thickness of approximately 5.1 nm and 4.8 nm per tetralayer deposited respectively (Figure 2b). At pH 5.0 assembly conditions, the PAA chains are less ionized, resulting in the deposition of thicker polyelectrolyte layers between the clay layers, decreasing the overall clay content of the film to approximately 38% (Table 1). This is a similar trend to what is observed in the literature for dipped (PAH/PAA) bilayer films over the same pH range[40]. Within the margin of error, the thickness of the tetralayer pH 5.0 film appears to be a linear sum of the LAP-containing bilayer and the (PAH/PAA) pH 5.0 bilayer, implying the intercalating clay layers do not have a significant impact on the dynamics on the polyelectrolyte deposition, unlike what has been observed for other LbL polymer-clay nanocomposite films[64]. There are two contributing factors that explain this observation. First,

the smaller LAP clay platelets form more uniform surface layers during each deposition cycle. Second, the short deposition times employed by the spray-LbL assembly process tend to generate linearly growing films, in contrast to the exponential growth patterns observed with weak polyelectrolytes assembled via dip-LbL.

Thermal Cross-linking. The tetralayer composite films were cross-linked to form amide bonds *via* uncatalyzed heating in a 175°C oven at atmospheric pressure for 5 hours. The resulting covalent bond formation was characterized by ATR-FTIR spectroscopy (Figure 3). Qualitatively, the 1550-1540 cm^{-1} peak corresponds to the N-H bending in the amine and is significantly reduced after cross-linking, indicating the reaction of primary amines to form secondary amides. Through the application of ORIGIN software for linear baseline adjustment, peak deconvolution, and peak integration, an estimate of roughly 20.6% of the amine groups were cross-linked for the pH 5.0 films (Figure 3a), compared to 12.8% for pH 6.0 films (Figure 3b). The increase in the degree of cross-linking for the pH 5.0 films is attributable to the increased number of free, unbounded acid functional groups present in the pH 5.0 films that are available at the lower pH of assembly. An additional side reaction possible with these free carboxylic acid groups is the formation of acid anhydrides. The formation of acid anhydride bonds was not observed; the key peaks for the identification of these bonds are in the 1830-1800 cm^{-1} and 1775-1740 cm^{-1} range, neither of which were appreciable in the spectra.

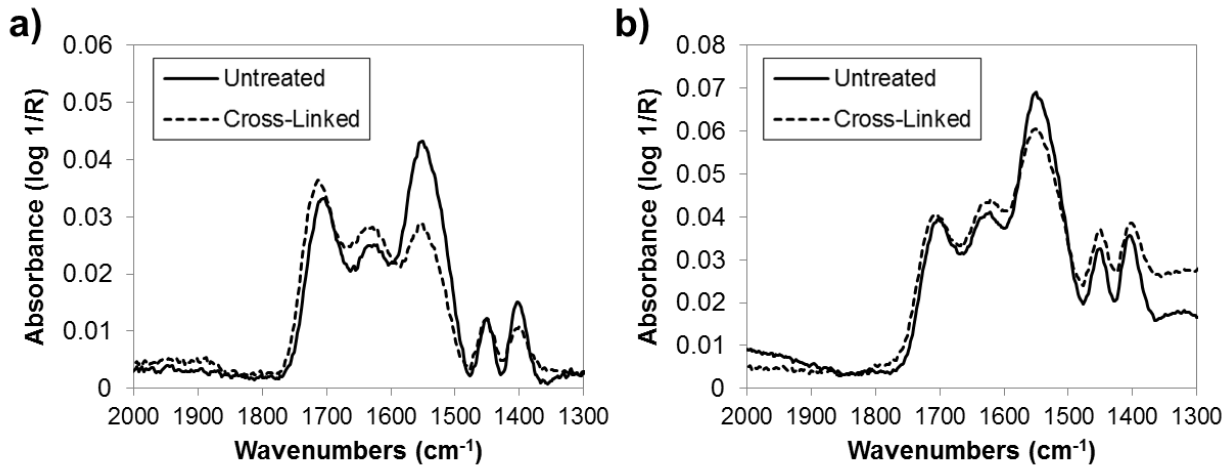

Figure 3. ATR-FTIR spectrograph showing the untreated films (solid line) and the films cross-linked at 175°C for 5 hr (dashed line) for (a) (PAH/PAA/PAH/LAP) pH 5.0 films, and for (b) (PAH/PAA/PAH/LAP) pH 6.0 films.

To show the impact of the cross-linking under aqueous conditions, spectroscopic ellipsometry was used on 20 bilayer and tetralayer samples to evaluate the degree of swelling in both in the untreated and cross-linked state (Table 2). The uncross-linked (PAH/PAA) pH 5.0 films were observed to significantly swell as the films undergo a significant pH shift from the assembly conditions as well as have more free amine and carboxylic acid groups present to form hydrogen bonds with water molecules. The composite bilayer of (PAH/LAP) swelled approximately 62% upon exposure to DI water, significantly less than the polyelectrolyte (PAH/PAA) pH 5.0 films. Cross-linking reduced the observed film swelling to roughly 10-15% regardless of assembly pH. This suggests that the covalent bonds formed during the cross-linking process both reduce the number of free amine and carboxylic acid groups that can interact with water and physically constrain the swelling of the film.

Table 2. Swelling in untreated and cross-linked films

Film Architecture	*Untreated*	*Cross-linked*
(PAH/LAP), pH 5	62% ± 5%	--
(PAH/PAA), pH 5	110% ± 38%	11% ± 13%
(PAH/PAA), pH 6	19% ± 2%	10% ± 10%
(PAH/PAA/PAH/LAP), pH 5	147% ± 3%	15% ± 3%
(PAH/PAA/PAH/LAP), pH 6	37% ± 2%	11% ± 1%

Imaging of Composite Films. The uncoated substrate, a polyethersulfone (PES) ultrafiltration membrane, has a regular distribution of surface pores of approximately 30 nm diameter (Figure 4a). Deposited film components, such as $(PAH/PAA/PAH/LAP)_{40}$ film architecture shown in Figure 4b, bridge the underlying pore structure to form thin, relatively smooth surface films. These films do not appear to penetrate into the underlying porous structure of the PES membrane, as observed by comparing the cross-sectional SEM micrographs for the uncoated membranes in Figure 4c and a $(PAH/PAA/PAH/LAP)_{40}$-coated membrane in Figure 4d. Clay platelets with intercalating polymer regions were observed by TEM imaging of the cross-sections of these membranes, shown in Figure 4e. Through ImageJ software analysis, the approximate size of the clay platelets observed in the cross-sectional SEM was on the order of 50 nm, indicating the clay platelets are not aggregated within the film and are intercalated within the polymer matrix. There was no statistically significant difference apparent in the average platelet spacing for the uncross-linked pH 5.0 films (2.41±0.23 nm) and the cross-linked films (2.57±0.39 nm).

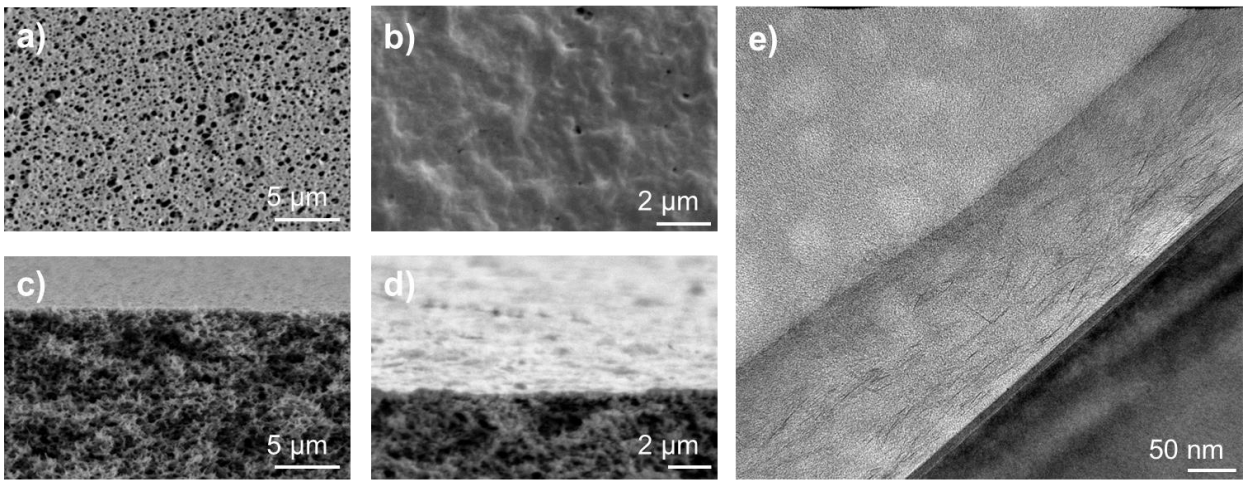

Figure 4. a) SEM micrograph of uncoated PES ultrafiltration membrane with 30 nm pores; b) SEM micrograph of $(PAH/PAA/PAH/LAP)_{40}$ pH 5.0 composite tetralayer film on PES membrane; c) cross-sectional SEM micrograph of uncoated PES membrane; d) cross-sectional SEM micrograph of $(PAH/PAA/PAH/LAP)_{40}$ pH 5.0 composite tetralayer film on PES membrane; and e) TEM micrograph of $(PAH/PAA/PAH/LAP)_{40}$ pH 5.0 composite tetralayer film deposited on Si wafer.

Micrographs were also taken of the membranes as assembled and after water and salt permeation experiments were conducted (Figure 5). Significant defects formed in $(PDAC/LAP)_{40}$ and $(PDAC/LAP)_{60}$ films following the permeation trials with applied pressures in excess of 100 psig (Figure 5a and 5b). Qualitatively, it would appear that matrix of the PDAC and LAP film formed during the LbL deposition process does not have the mechanical cohesiveness and integrity to withstand the *in situ* RO conditions. The cross-linked $(PAH/PAA/PAH/LAP)_{40}$ and $(PAH/PAA/PAH/LAP)_{60}$ films however, do not exhibit such defects after permeation trials (Figure 5c and 5d), indicating the covalently bonded LbL film is more mechanically robust under RO conditions. Salt deposits in the form of micron-sized salt crystals were observed on the surfaces of LbL films following the permeation trials, however

these crystals appear independently of the fractures in the (PDAC/LAP) films and are the result of the washing and drying of the films in the sample preparation for the SEM.

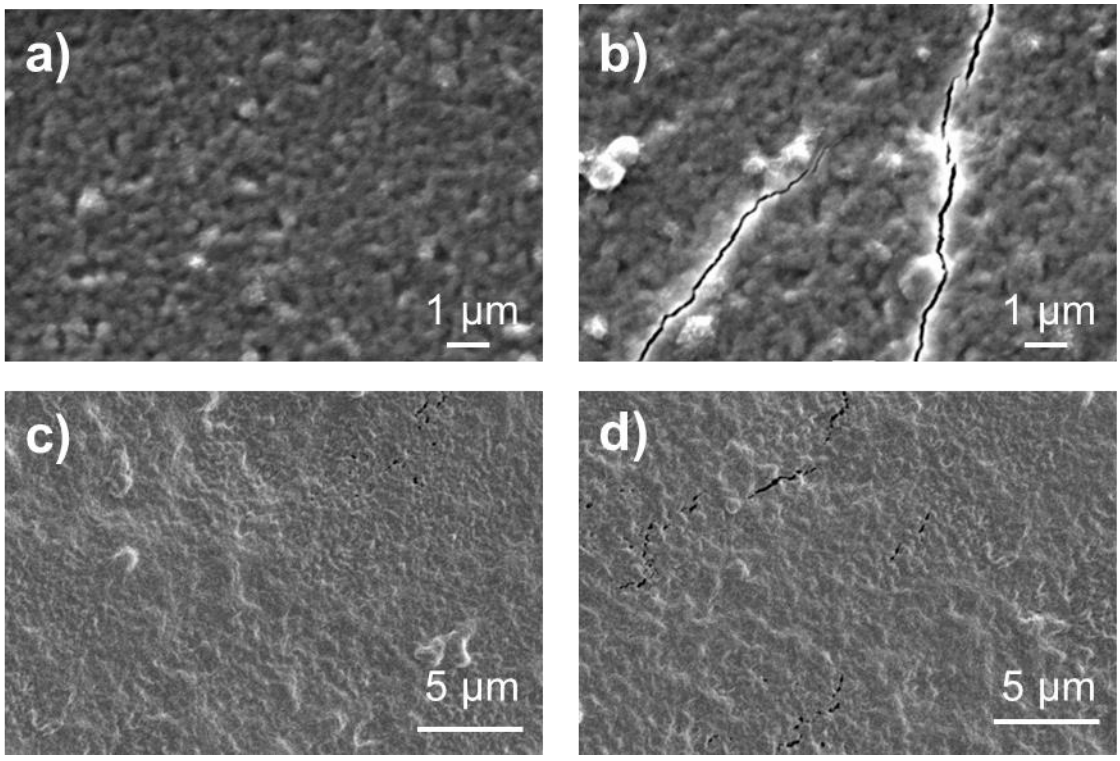

Figure 5. a) SEM micrograph of $(PDAC/LAP)_{40}$ 3s:3s film as prepared before permeation experiments; b) SEM micrograph of $(PDAC/LAP)_{40}$ 3s:3s film after water and salt permeation experiments; c) SEM micrograph of $(PAH/PAA/PAH/LAP)_{40}$ pH 5.0 film as prepared before permeation experiments; d) SEM micrograph of $(PAH/PAA/PAH/LAP)_{40}$ pH 5.0 after water and salt permeation experiments.

Permeation Properties of LbL Films. Water flux and salt rejection data on the thin films were collected from dead-end permeation cell measurements over a pressure range of 50 psig to 250 psig with 10,000 ppm NaCl solution (Figure 6a and 6b respectively). A localized permeability coefficient was calculated through a regression of the Spiegler-Kedem model to

yield a single value to compare films where several different transport mechanisms are at work. The water permeability of the commercial TFC-HR polyamide active layer under these operating conditions is $7.6 \cdot 10^{-15}$ m^2 / Pa s with 98% salt rejection. All the examined LbL films exhibited significantly greater water permeability, on the order of one to two orders of magnitude.

Due to the formation of defects in the (PDAC/LAP) selective layers, the salt rejection was low: 28% for the 3s:3s film and 10% for the 3s:9s film. The water permeability for the 3s:3s film was $2.27 \cdot 10^{-13}$ m^2 / Pa s and for the 3s:9s film $8.96 \cdot 10^{-13}$ m^2 / Pa s, roughly four times greater. It is likely that the lower salt rejection and increased water flux correspond to an increase in the cracks formed in the (PDAC/LAP) films during operation (Figure 5). However, this phenomenon appears to have been eliminated in the tetralayer composite films, which exhibit similar water permeability but significantly increased salt rejection.

It is notable that for the composite tetralayer series from pH 6.0 to 5.0, the water permeability dropped by approximately a factor of two from $4.60 \cdot 10^{-13}$ m^2 / Pa s to $2.82 \cdot 10^{-13}$ m^2 / Pa s. However, the salt rejection increased from an average of 46% to 89%. We suspect this occurs for two reasons: 1) the increased degree of cross-linking in pH 5.0 films reduces the effective averaged channel width between clay layers after swelling under *in situ* RO conditions, and 2) additional free carboxylic acid groups present in the pH 5.0 film slow the diffusion of solvated ions due to charge effects. The ultimate impact of these two phenomena is an increase in tortuosity of the selective layer, resulting in longer diffusive path lengths for solvated ions.

It is also notable that the overall clay content of the film does not directly correlate to its performance in the salt rejection trials. The best performing film, the (PAH/PAA/PAH/LAP) pH 5.0 film, had an average clay content of 38% and a salt rejection of 89%. Extremely high clay

content films assembled via the (PDAC/LAP) method perform similarly with regards to water permeation, but were more brittle due to the high clay content, and thus more susceptible to critical defect formation during RO, with a 83% clay membrane only rejecting 10% of salt ions. This demonstrates the importance of the cross-linked polymeric matrix that reduces the brittleness of the film; these cross-links fortify the polymeric matrix encompassing the clay platelets, and prevent the formation of cracking and critical faults under *in situ* RO conditions. The film architecture without clay, the (PAH/PAA) bilayer architecture, only exhibited 53% salt rejection. This is indicative of a swollen polymeric matrix that does not serve as an effective barrier to solvated ion diffusion due to the lack of size exclusion-driven rejection through the nano-channels present in the clay composite films. To better illustrate the trade-off between increased water permeability and salt rejection, the salt and water permeation data is plotted against each other (Figure 6c).

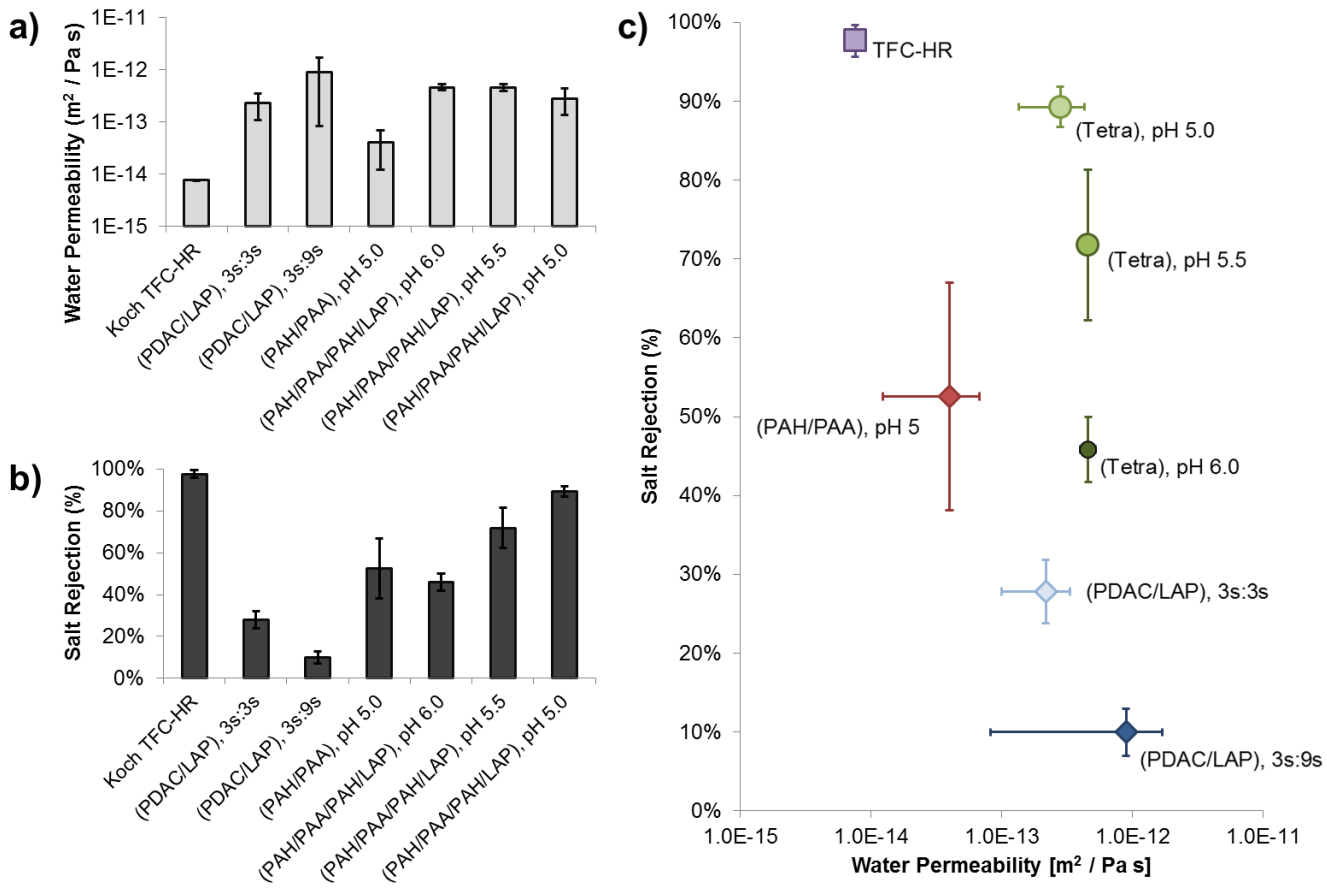

Figure 6. Plot of (a) water permeability of layer-by-layer thin films against commercially-available Koch TFC-HR RO membrane, (b) salt rejection of layer-by-layer thin films against commercially-available Koch TFC-HR RO membrane, and (c) prior data plotted on two-axis graph of water permeability against salt rejection.

Conclusion

In this report, we have demonstrated the effectiveness of using LAP clay in spray-LbL assembled selective layers for RO membranes in both a strong polyelectrolyte film architecture, (PDAC/LAP), and a weak polyelectrolyte film architecture, (PAH/PAA/PAH/LAP). The physical and permeability properties of these two architectures were characterized and compared.

The calculated water permeability through the Spiegler-Kedem model for all LbL-assembled composite thin films was between one and two orders of magnitude greater than what was observed for commercially-available thin film composite RO membranes. The salt rejection measured for un-crosslinked bilayer (PDAC/LAP) films was between 10% and 28% and for the cross-linked tetralayer (PAH/PAA/PAH/LAP) films was between 46% and 89%, with the greatest salt rejection observed for films assembled at pH 5.0.

The (PDAC/LAP) composite bilayer film architectures were too brittle under *in situ* RO conditions and formed critical defects during operation. These defects were effectively eliminated by the introduction of a cross-linkable polymer matrix of PAH and PAA that reduced brittleness and film swelling under aqueous conditions, which made the composite films more mechanically tough and maintained the nano-channels between platelet layers. We hypothesize that the selective salt rejection and high water permeability is the result of a combination of two transport mechanisms: a size-exclusion transport mechanism that hinders the flow of solvated ions between clay layers to a greater degree than individual water molecules, and charge interactions between the polyelectrolytes and the solvated ions in the selective layer. We attribute the efficacy of the pH 5.0 tetralayer architecture over the pH 6.0 to the increased degree of cross-linking via free carboxylic acid groups which strengthens the polymeric matrix, as well as the enhanced presence of free carboxylic acid groups that may act as hydrated regions to further enhance water permeability while retarding ion transport.

Interestingly, although the (PDAC/LAP) films have higher clay content than the tetralayer (PAH/PAA/PAH/LAP) films and naively one would predict a greater degree of tortuosity for these films leading to an increase in salt selectivity, a more complicated trend was observed. This was due to the high rate of defect formation observed for the (PDAC/LAP)

bilayer films under RO conditions, which was reduced through increasing the polymer content of the film and forming a strong polymeric matrix through thermal cross-linking. However, given the polymer (PAH/PAA) bilayer films exhibited 53% salt rejection, there is necessarily an optimal value for maximizing salt rejection as a function of clay content. Of the film architectures investigated, the best performing film was tetralayer pH 5.0 film with an average clay content of 38%, a degree of incorporation that is difficult to achieve with other assembly methods but is attainable through spray-LbL assembly.

These findings represent an opportunity for further development of LbL-assembled clay composite formulations that can be adapted to water filtration applications. Furthermore, if the fouling properties were characterized or dedicated antifouling layers were introduced, these high-flux clay composite membranes could provide a high throughput alternative for wastewater and brackish water treatment and potentially for forward osmosis applications.

Experimental Section

Materials. Laponite clay was provided by Southern Clay Products; clay dispersions were prepared at a concentration of 1.0 wt.% clay and the balance reagent-grade water. Poly(diallyldimethylammonium chloride) (MW: 200-350 kDa) was obtained from Sigma-Aldrich, and both poly(allylamine hydrochloride) (MW: 60 kDa) and poly(acrylic acid) (MW: 20 kDa) were obtained from Polysciences, Inc. Polyelectrolyte solutions were prepared at 10 mM concentration and were adjusted to the assembly pH by using a Φ340 pH/Temp Meter and concentrated HCl or NaOH solution as appropriate. Millipore PES ultrafiltration membranes with 30 nm pores were purchased and used as a substrate for deposition. PES membranes were

plasma-cleaned in a Harrick Plasma Cleaner/Sterilizer PDC-32G at 18 W for 30 seconds and soaked in PDAC or PAH solutions before spray-LbL film assembly.

Spray Layer-by-Layer (Spray-LbL) Deposition. Films were constructed using a custom-built spraying apparatus. Solutions and clay dispersions were aerosolized with N_2 gas at 20 psi and are sprayed onto the substrate rotated at 10 rpm. The basic program for each layer involved spraying the film component for 3 seconds, pausing for a 5 second drain period, rinsing for 10 seconds with pH-adjusted water, and then and then a final 5 second drain period. The sequence is repeated for each film component listed to assemble a bilayer or tetralayer. Films assembled at different component spray times are identified by the expression ns:ms, where n refers to the spray time of PDAC, and m refers to the spray time of LAP.

Characterization. A Dektak 150 profilometer was used to determine the film thickness. Profilometry samples were deposited on glass slides plasma-cleaned using the above equipment for 5 minutes; otherwise, the standard protocol above was used. Both a JEOL JSM-6060 and a JSM-6010LA Scanning Electron Microscopes (SEM) were used to image both film surfaces and cross-sections. Cross-sectional SEM samples were prepared via the cryo-fracture method by submerging the sample in liquid N2 and then physically separated. A J.A. Woollam Co., Inc. M-2000D spectroscopic ellipsometer was used to determine swelling through the measured change in film thickness between the dry state and being immersed in DI water for films deposited on Si wafers. The spectra were fitted with a 1) Si model, 2) SiO_2 model, and 3) Cauchy model corresponding to 1) the bulk of the Si wafer, 2) the oxidized surface of the Si wafer, and 3) the LbL-deposited thin film. A TA Instruments Discovery Series Thermogravimetric Analyzer was used to determine the film composition of LbL films (150-200 bilayer/tetralayer depositions on polystyrene chips) with the following program: temperature equilibration step at 65 °C for 5

minutes, followed by a ramp up to 800 °C at the rate of 10 °C/min, followed by a final temperature equilibration step at 800 °C for 5 minutes. The percentage clay content was calculated by taking the final mass of the remaining film after thermal decomposition and dividing by the mass taken after the temperature equilibriation step at 65 °C. A Sterlitech HP4750 dead-end permeation cell was used to determine both water permeability and salt rejection. The cell was operated with an applied pressure between 50 and 300 psi and on a Benchmark H4000-S-E Magnetic Stirrer at speed '8' for films assembled on ultrafiltration membranes. A Spiegler-Kedem model was applied to determine the local water permeability constants. The chloride ion concentration of the collected permeate was measured with an Oakton Ion 700 conductivity meter and Thermo-Scientific Orion 9617BNWP IonPlus Probe.

ASSOCIATED CONTENT

Supporting Information. The method for calculating water permeability via the Spiegler-Kedem method, a pore size distribution analysis on the PES-30 nm UF membranes, and nanoindentation testing on a selection of films from this report are available in the supplemental information.

AUTHOR INFORMATION

Corresponding Author

*Email: hammond@mit.edu.

Author Contributions

The manuscript was written through contributions of all authors. All authors have given approval to the final version of the manuscript.

Notes

The authors declare no competing financial interest.

ACKNOWLEDGMENT

The authors would like to thank the Center for Clean Water and Clean Energy at MIT and KFUPM under Project #R5-CW-08 for funding the work presented. The Institute for Soldier Nanotechnologies (ISN) at MIT is gratefully acknowledged for providing laboratory space and equipment.

ABBREVIATIONS

LAP, laponite clay; LbL, layer-by-layer; PAA, poly(acrylic acid); PAH, poly(allylamine); PDAC, poly(diallyldimethylammonium chloride); PES, poly(ethersulfone); RO, reverse osmosis; spray-LbL, spray layer-by-layer

REFERENCES

1. Gleick, P. H., *The World's Water: The Biennial Report on Freshwater Resources*. Island Press: Washington, DC, **2014**; Vol. 8.
2. Pereira, L. S.; Oweis, T.; Zairi, A., Irrigation Management under Water Scarcity. *Agricultural Water Management* **2002,** *57*, 175-206.
3. Qadir, M.; Oster, J. D., Crop and Irrigation Management Strategies for Saline-Sodic Soils and Waters Aimed at Environmentally Sustainable Agriculture. *Sci. Total Environ.* **2004,** *323*, 1-19.
4. Dudka, S.; Adriano, D. C., Environmental Impacts of Metal Ore Mining and Processing: A Review. *J. Environ. Qual.* **1997,** *26*, 590-602.
5. Akcil, A.; Koldas, S., Acid Mine Drainage (Amd): Causes, Treatment and Case Studies. *J. Cleaner Prod.* **2006,** *14*, 1139-1145.
6. Nagajyoti, P. C.; Lee, K. D.; Sreekanth, T. V. M., Heavy Metals, Occurrence and Toxicity for Plants: A Review. *Environ. Chem. Lett.* **2010,** *8*, 199-216.
7. Lee, J.; Mahendra, S.; Alvarez, P. J. J., Nanomaterials in the Construction Industry: A Review of Their Applications and Environmental Health and Safety Considerations. *ACS Nano* **2010,** *4*, 3580-3590.
8. Sipma, J.; Osuna, M. B.; Emanuelsson, M. A. E.; Castro, P. M. L., Biotreatment of Industrial Wastewaters under Transient-State Conditions: Process Stability with Fluctuations of

Organic Load, Substrates, Toxicants, and Environmental Parameters. *Crit. Rev. Environ. Sci. Technol.* **2010,** *40*, 147-197.
9. Foley, J. A.; DeFries, R.; Asner, G. P.; Barford, C.; Bonan, G.; Carpenter, S. R.; Chapin, F. S.; Coe, M. T.; Daily, G. C.; Gibbs, H. K.; Helkowski, J. H.; Holloway, T.; Howard, E. A.; Kucharik, C. J.; Monfreda, C.; Patz, J. A.; Prentice, I. C.; Ramankutty, N.; Snyder, P. K., Global Consequences of Land Use. *Science* **2005,** *309*, 570-574.
10. Greenlee, L. F.; Lawler, D. F.; Freeman, B. D.; Marrot, B.; Moulin, P., Reverse Osmosis Desalination: Water Sources, Technology, and Today's Challenges. *Water Res.* **2009,** *43*, 2317-2348.
11. Semiat, R., Energy Issues in Desalination Processes. *Environ. Sci. Technol.* **2008,** *42*, 8193-8201.
12. Lee, K. P.; Arnot, T. C.; Mattia, D., A Review of Reverse Osmosis Membrane Materials for Desalination-Development to Date and Future Potential. *J. Membr. Sci.* **2011,** *370*, 1-22.
13. Song, L. F.; Hu, J. Y.; Ong, S. L.; Ng, W. J.; Elimelech, M.; Wilf, M., Emergence of Thermodynamic Restriction and Its Implications for Full-Scale Reverse Osmosis Processes. *Desalination* **2003,** *155*, 213-228.
14. Petersen, R. J., Composite Reverse Osmosis and Nanofiltration Membranes. *J. Membr. Sci.* **1993,** *83*, 81-150.
15. Wang, J.; Dlamini, D. S.; Mishra, A. K.; Pendergast, M. T. M.; Wong, M. C. Y.; Mamba, B. B.; Freger, V.; Verliefde, A. R. D.; Hoek, E. M. V., A Critical Review of Transport through Osmotic Membranes. *J. Membr. Sci.* **2014,** *454*, 516-537.
16. Welty, J.; Wicks, C. E.; Rorrer, G. L.; Wilson, R. E., *Fundamentals of Momentum, Heat and Mass Transfer*. Wiley: **2007**.
17. Wolynes, P. G., Molecular Theory of Solvated Ion Dynamics. *J. Chem. Phys.* **1978,** *68*, 473-483.
18. Chen, J. H.; Adelman, S. A., Macroscopic Model for Solvated Ion Dynamics. *J. Chem. Phys.* **1980,** *72*, 2819-2831.
19. Eliad, L.; Salitra, G.; Soffer, A.; Aurbach, D., Ion Sieving Effects in the Electrical Double Layer of Porous Carbon Electrodes: Estimating Effective Ion Size in Electrolytic Solutions. *J. Phys. Chem. B* **2001,** *105*, 6880-6887.
20. Marcus, Y., Ionic Radii in Aqueous Solutions. *Chem. Rev.* **1988,** *88*, 1475-1498.
21. Rips, I.; Klafter, J.; Jortner, J., Dynamics of Ionic Solvation. *J. Chem. Phys.* **1988,** *88*, 3246-3252.
22. Humplik, T.; Lee, J.; O'Hern, S. C.; Fellman, B. A.; Baig, M. A.; Hassan, S. F.; Atieh, M. A.; Rahman, F.; Laoui, T.; Karnik, R.; Wang, E. N., Nanostructured Materials for Water Desalination. *Nanotechnology* **2011,** *22*.
23. Fornasiero, F.; Park, H. G.; Holt, J. K.; Stadermann, M.; Grigoropoulos, C. P.; Noy, A.; Bakajin, O., Ion Exclusion by Sub-2-Nm Carbon Nanotube Pores. *Proc. Natl. Acad. Sci. U. S. A.* **2008,** *105*, 17250-17255.
24. Cohen-Tanugi, D.; Grossman, J. C., Water Desalination across Nanoporous Graphene. *Nano Lett.* **2012,** *12*, 3602-3608.
25. Balta, S.; Sotto, A.; Luis, P.; Benea, L.; Van der Bruggen, B.; Kim, J., A New Outlook on Membrane Enhancement with Nanoparticles: The Alternative of Zno. *J. Membr. Sci.* **2012,** *389*, 155-161.
26. Lee, H. S.; Im, S. J.; Kim, J. H.; Kim, H. J.; Kim, J. P.; Min, B. R., Polyamide Thin-Film Nanofiltration Membranes Containing Tio2 Nanoparticles. *Desalination* **2008,** *219*, 48-56.

27. Jeong, B. H.; Hoek, E. M. V.; Yan, Y. S.; Subramani, A.; Huang, X. F.; Hurwitz, G.; Ghosh, A. K.; Jawor, A., Interfacial Polymerization of Thin Film Nanocomposites: A New Concept for Reverse Osmosis Membranes. *J. Membr. Sci.* **2007,** *294*, 1-7.
28. Kim, W. G.; Nair, S., Membranes from Nanoporous 1d and 2d Materials: A Review of Opportunities, Developments, and Challenges. *Chem. Eng. Sci.* **2013,** *104*, 908-924.
29. Adhikari, M.; Ghosh, S. K., Microporous Clay Membrane Materials for Reverse-Osmosis Applications .1. Performance-Characteristics from Osmotic Studies. *J. Appl. Polym. Sci.* **1989,** *37*, 1125-1136.
30. Abbasi, M.; Salahi, A.; Mirfendereski, M.; Mohammadi, T.; Rekabdar, F.; Hemmati, M., Oily Wastewater Treatment Using Mullite Ceramic Membrane. *Desalin. Water Treat.* **2012,** *37*, 21-30.
31. Jang, W. S.; Rawson, I.; Grunlan, J. C., Layer-by-Layer Assembly of Thin Film Oxygen Barrier. *Thin Solid Films* **2008,** *516*, 4819-4825.
32. Priolo, M. A.; Gamboa, D.; Grunlan, J. C., Transparent Clay-Polymer Nano Brick Wall Assemblies with Tailorable Oxygen Barrier. *ACS Appl. Mater. Interfaces* **2010,** *2*, 312-320.
33. Laufer, G.; Kirkland, C.; Cain, A. A.; Grunlan, J. C., Clay-Chitosan Nanobrick Walls: Completely Renewable Gas Barrier and Flame-Retardant Nanocoatings. *ACS Appl. Mater. Interfaces* **2012,** *4*, 1643-1649.
34. Priolo, M. A.; Holder, K. M.; Greenlee, S. M.; Stevens, B. E.; Grunlan, J. C., Precisely Tuning the Clay Spacing in Nanobrick Wall Gas Barrier Thin Films. *Chem. Mater.* **2013,** *25*, 1649-1655.
35. Gaskell, E. E.; Hamilton, A. R., Antimicrobial Clay-Based Materials for Wound Care. *Future Med. Chem.* **2014,** *6*, 641-655.
36. Hsu, S.-h.; Wang, M.-C.; Lin, J.-J., Biocompatibility and Antimicrobial Evaluation of Montmorillonite/Chitosan Nanocomposites. *Appl. Clay Sci.* **2012,** *56*, 53-62.
37. Katti, K. S.; Ambre, A. H.; Peterka, N.; Katti, D. R., Use of Unnatural Amino Acids for Design of Novel Organomodified Clays as Components of Nanocomposite Biomaterials. *Philos. Trans. R. Soc., A* **2010,** *368*, 1963-1980.
38. Lvov, Y.; Abdullayev, E., Functional Polymer-Clay Nanotube Composites with Sustained Release of Chemical Agents. *Prog. Polym. Sci.* **2013,** *38*, 1690-1719.
39. Decher, G., Fuzzy Nanoassemblies: Toward Layered Polymeric Multicomposites. *Science* **1997,** *277*, 1232-1237.
40. Shiratori, S. S.; Rubner, M. F., Ph-Dependent Thickness Behavior of Sequentially Adsorbed Layers of Weak Polyelectrolytes. *Macromolecules* **2000,** *33*, 4213-4219.
41. Bertrand, P.; Jonas, A.; Laschewsky, A.; Legras, R., Ultrathin Polymer Coatings by Complexation of Polyelectrolytes at Interfaces: Suitable Materials, Structure and Properties. *Macromol. Rapid Commun.* **2000,** *21*, 319-348.
42. Krogman, K. C.; Zacharia, N. S.; Schroeder, S.; Hammond, P. T., Automated Process for Improved Uniformity and Versatility of Layer-by-Layer Deposition. *Langmuir* **2007,** *23*, 3137-3141.
43. Jin, W. Q.; Toutianoush, A.; Tieke, B., Use of Polyelectrolyte Layer-by-Layer Assemblies as Nanofiltration and Reverse Osmosis Membranes. *Langmuir* **2003,** *19*, 2550-2553.
44. Malaisamy, R.; Bruening, M. L., High-Flux Nanofiltration Membranes Prepared by Adsorption of Multilayer Polyelectrolyte Membranes on Polymeric Supports. *Langmuir* **2005,** *21*, 10587-10592.

45. Qiu, C. Q.; Qi, S. R.; Tang, C. Y. Y., Synthesis of High Flux Forward Osmosis Membranes by Chemically Crosslinked Layer-by-Layer Polyelectrolytes. *J. Membr. Sci.* **2011,** *381*, 74-80.
46. Park, J.; Park, J.; Kim, S. H.; Cho, J.; Bang, J., Desalination Membranes from Ph-Controlled and Thermally-Crosslinked Layer-by-Layer Assembled Multilayers. *J. Mater. Chem.* **2010,** *20*, 2085-2091.
47. Fadhillah, F.; Zaidi, S. M. J.; Khan, Z.; Khaled, M. M.; Rahman, F.; Hammond, P. T., Development of Polyelectrolyte Multilayer Thin Film Composite Membrane for Water Desalination Application. *Desalination* **2013,** *318*, 19-24.
48. Hoffmann, K.; Friedrich, T.; Tieke, B., Layer-by-Layer Assembled Polyelectrolyte Blend Membranes and Their Use for Ion Separation and Rejection. *Polym. Eng. Sci.* **2011,** *51*, 1497-1506.
49. Gu, J. E.; Lee, S.; Stafford, C. M.; Lee, J. S.; Choi, W.; Kim, B. Y.; Baek, K. Y.; Chan, E. P.; Chung, J. Y.; Bang, J.; Lee, J. H., Molecular Layer-by-Layer Assembled Thin-Film Composite Membranes for Water Desalination. *Adv. Mater.* **2013,** *25*, 4778-4782.
50. El-Hashani, A.; Toutianoush, A.; Tieke, B., Use of Layer-by-Layer Assembled Ultrathin Membranes of Dicopper- 18 Azacrown-N-6 Complex and Polyvinylsulfate for Water Desalination under Nanofiltration Conditions. *J. Membr. Sci.* **2008,** *318*, 65-70.
51. Kleinfeld, E. R.; Ferguson, G. S., Stepwise Formation of Multilayered Nanostructural Films from Macromolecular Precursors. *Science* **1994,** *265*, 370-373.
52. Eckle, M.; Decher, G., Tuning the Performance of Layer-by-Layer Assembled Organic Light Emitting Diodes by Controlling the Position of Isolating Clay Barrier Sheets. *Nano Lett.* **2001,** *1*, 45-49.
53. Glinel, K.; Laschewsky, A.; Jonas, A. M., Ordered Polyelectrolyte "Multilayers". 3. Complexing Clay Platelets with Polycations of Varying Structure. *Macromolecules* **2001,** *34*, 5267-5274.
54. Choudalakis, G.; Gotsis, A. D., Permeability of Polymer/Clay Nanocomposites: A Review. *Eur. Polym. J.* **2009,** *45*, 967-984.
55. Lutkenhaus, J. L.; Olivetti, E. A.; Verploegen, E. A.; Cord, B. M.; Sadoway, D. R.; Hammond, P. T., Anisotropic Structure and Transport in Self-Assembled Layered Polymer-Clay Nanocomposites. *Langmuir* **2007,** *23*, 8515-8521.
56. Yang, Y. H.; Malek, F. A.; Grunlan, J. C., Influence of Deposition Time on Layer-by-Layer Growth of Clay-Based Thin Films. *Ind. Eng. Chem. Res.* **2010,** *49*, 8501-8509.
57. Pavlidou, S.; Papaspyrides, C. D., A Review on Polymer-Layered Silicate Nanocomposites. *Prog. Polym. Sci.* **2008,** *33*, 1119-1198.
58. Alexandre, M.; Dubois, P., Polymer-Layered Silicate Nanocomposites: Preparation, Properties and Uses of a New Class of Materials. *Mater. Sci. Eng., R* **2000,** *28*, 1-63.
59. Nicolai, T.; Cocard, S., Light Scattering Study of the Dispersion of Laponite. *Langmuir* **2000,** *16*, 8189-8193.
60. Shalkevich, A.; Stradner, A.; Bhat, S. K.; Muller, F.; Schurtenberger, P., Cluster, Glass, and Gel Formation and Viscoelastic Phase Separation in Aqueous Clay Suspensions. *Langmuir* **2007,** *23*, 3570-3580.
61. Harris, J. J.; DeRose, P. M.; Bruening, M. L., Synthesis of Passivating, Nylon-Like Coatings through Cross-Linking of Ultrathin Polyelectrolyte Films. *J. Am. Chem. Soc.* **1999,** *121*, 1978-1979.

62. Podsiadlo, P.; Kaushik, A. K.; Arruda, E. M.; Waas, A. M.; Shim, B. S.; Xu, J. D.; Nandivada, H.; Pumplin, B. G.; Lahann, J.; Ramamoorthy, A.; Kotov, N. A., Ultrastrong and Stiff Layered Polymer Nanocomposites. *Science* **2007,** *318*, 80-83.
63. Cranford, S. W.; Ortiz, C.; Buehler, M. J., Mechanomutable Properties of a Paa/Pah Polyelectrolyte Complex: Rate Dependence and Ionization Effects on Tunable Adhesion Strength. *Soft Matter* **2010,** *6*, 4175-4188.
64. Priolo, M. A.; Gamboa, D.; Holder, K. M.; Grunlan, J. C., Super Gas Barrier of Transparent Polymer-Clay Multi Layer Ultrathin Films. *Nano Lett.* **2010,** *10*, 4970-4974.